Research Article | Vol. 31, No. 6 / 13 Mar 2023 / Optics Express 10297
Optics EXPRESS

# Fano asymmetry in zero–detuned exciton–plasmon systems

ÁLVARO NODAR,[1,2] TOMAS NEUMAN,[3] YAO ZHANG,[4] JAVIER AIZPURUA,[1,2] AND RUBEN ESTEBAN[1,2,*]

[1]Centro de Física de Materiales CFM-MPC (CSIC-UPV/EHU), San Sebastián-Donostia, 20018, Spain
[2]Donostia International Physics Center (DIPC) San Sebastián-Donostia, 20018, Spain
[3]Institut des Sciences Moléculaires d'Orsay (ISMO), UMR 8214, CNRS, Université Paris-Saclay, 91405 Orsay Cedex, France
[4]Hefei National Research Center for Physical Sciences at the Microscale and Synergetic Innovation Centre of Quantum Information and Quantum Physics, University of Science and Technology of China, Hefei 230026, Anhui, China
*ruben.esteban@ehu.eus

**Abstract:** Plasmonic resonances in metallic nanostructures can strongly enhance the emission from quantum emitters, as commonly used in surface-enhanced spectroscopy techniques. The extinction and scattering spectrum of these quantum emitter-metallic nanoantenna hybrid systems are often characterized by a sharp Fano resonance, which is usually expected to be symmetric when a plasmonic mode is resonant with an exciton of the quantum emitter. Here, motivated by recent experimental work showing an asymmetric Fano lineshape under resonant conditions, we study the Fano resonance found in a system composed of a single quantum emitter interacting resonantly with a single spherical silver nanoantenna or with a dimer nanoantenna composed of two gold spherical nanoparticles. To analyze in detail the origin of the resulting Fano asymmetry we develop numerical simulations, an analytical expression that relates the asymmetry of the Fano lineshape to the field enhancement and to the enhanced losses of the quantum emitter (Purcell effect), and a set of simple models. In this manner we identify the contributions to the asymmetry of different physical phenomena, such as retardation and the direct excitation and emission from the quantum emitter.



## 1. Introduction

Plasmonic resonances supported by metallic nanoantennas can confine light to hot spots of extremely small effective volumes (of the order of $\sim 10$ nm$^3$) [1–5], leading to very efficient interaction with quantum emitters, such as quantum dots, solid-state color centers, or molecules. This interaction can modify the optical properties of the optical transition of a quantum emitter (QE), for example enhancing its emission rate, which can be exploited in a variety of applications in nanophotonics [6–8]. For example, in surface-enhanced spectroscopy, the coupling with the plasmonic nanoantennas enables the optical characterization of very small amounts or even single molecules [3,4,9–17]. Other applications include quantum information processing [18,19], biosensing [20,21], or the enhancement of optical non-linearities [22–24].

In this context, the elastic response of QEs interacting with nanoantennas often results in a distinctive narrow spectral feature, the so-called Fano resonance, that has been characterized in many different nanophotonic systems [14,25–32]. The Fano resonance can consist in a symmetric dip in the spectrum or in a very asymmetric lineshape [11,13,33–35]. It is generally well understood that the asymmetry of the Fano features depends strongly on the detuning between the resonance of the QEs and that of the plasmonic nanoantenna. A symmetric Fano dip is typically expected when the detuning of the QE and the nanoantenna resonances is zero (resonant system), and it becomes increasingly asymmetric as the detuning is increased [10–13]. However, it has

#477200 https://doi.org/10.1364/OE.477200
Journal © 2023 Received 3 Oct 2022; revised 17 Jan 2023; accepted 19 Jan 2023; published 7 Mar 2023

Optics EXPRESS

been recently emphasized [14] that clear asymmetric Fano lineshapes can also be found for zero detuning. In this paper, we analyze in detail the origin of the additional asymmetry of the Fano lineshape in the spectra of resonant plasmon-exciton systems. We consider an exciton of a single QE in resonance with an optical mode of a metallic nanoantenna, but the conclusions can be extended to other similar systems.

In this study, we first focus (sections 2–3) on the extinction cross-section spectrum of a silver spherical nanoparticle interacting resonantly with a QE. We first introduce a simple model that identifies why a symmetric Fano feature is typically expected under resonant conditions [10–13], and then we use rigorous electromagnetic calculations to show that an asymmetry in the spectrum can be present in a realistic configuration. The different phenomena that lead to the asymmetry are introduced and analyzed in detail in section 3, where we first develop an analytical expression that decomposes the Fano asymmetry factor into two different contributions. Furthermore, we implement a series of simple models to analyze how the Fano asymmetry is influenced by different aspects in the nanoantenna-QE interaction, such as retardation, direct illumination and emission of the QE, and the contribution to the dielectric permittivity of the nanoantenna from the band structure of $d$-electrons. Finally, in section 4 we illustrate the general validity of our study by analyzing a more complex nanoantenna, a dimer composed of two spherical gold nanoparticles. This study can help to better understand the asymmetry in Fano features beyond the detuning between exciton and plasmon resonances.

## 2. Fano asymmetry under resonant conditions

To illustrate why a symmetric Fano dip is expected under resonant conditions of excitation of a nanoantenna and a QE, and to expose how this expectation is not always fulfilled, we first compare i) the extinction cross-section of a canonical nanoantenna-QE system obtained using a simple model that results in a symmetric Fano dip with ii) the exact calculations giving an asymmetric Fano lineshape. We consider a silver spherical nanoparticle (nanoantenna) of radius $r = 20$ nm coupled to a QE under weak illumination. We treat the QE as a point-like dipole, representing an excitonic transition with polarizability along the direction perpendicular to the surface of the plasmonic nanoantenna ($x$-axis). The dipolar plasmon mode of the nanoantenna and the excitonic transition of the QE are resonant at the same wavelength $\lambda_0$ (frequency $\omega_0 = 2\pi c_0/\lambda_0$, with $c_0$ the speed of light in vacuum). The system is situated in a vacuum, and it is excited by a plane wave of amplitude $E_0$ polarized parallel to the dipole orientation (Fig. 1(a)).

To obtain the extinction spectrum of the hybrid QE-nanoantenna system, we first consider a simple dipole-dipole interaction model that treats the spherical nanoantenna as a second point-like dipole positioned at its center, representing the dipolar plasmon mode. In typical plasmonic systems, the fields induced by the nanoantenna at the position of the QE are much larger than the incident field [3,9], so that the direct illumination of the QE can be neglected. Using this assumption and the quasistatic approximation, we obtain the following coupled equations for the dipole moments (oriented along the $x$-axis) induced in the QE, $p_e$, and in the nanoantenna, $p_a$:

$$p_e = \alpha_e G^{qs}_{x,x} p_a, \tag{1}$$

$$p_a = \alpha_a (E_0 + G^{qs}_{x,x} p_e), \tag{2}$$

with $\alpha_a$ and $\alpha_e$ the polarizability of the nanoantenna and of the QE, respectively, and $G^{qs}_{x,x}$ the $\{x,x\}$–component of the quasistatic Green's function, which describes the field propagation between dipoles. Within a Drude model description of the permittivity of the metal and using a Drude-Lorentz model for the optical response of the QE, the $\alpha_e$ and $\alpha_a$ polarizabilities become:

$$\alpha_e = \frac{A_e}{\omega_0^2 - \omega^2 - i\gamma\omega}, \tag{3}$$

Optics EXPRESS

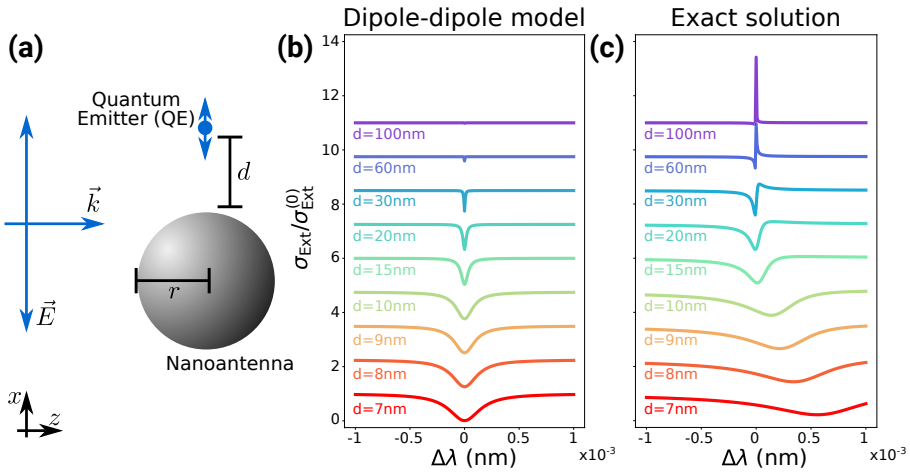


**Fig. 1.** Fano asymmetry under resonant nanoantenna-QE conditions. (a) Scheme of the system studied in sections 2–3. A QE is placed at a distance $d$ from the surface of a silver spherical nanoparticle of radius $r$. An excitonic transition couples resonantly with the dipolar mode of the nanoparticle. The excitonic transition in the QE is polarized along the $x$-axis that joins the center of the nanoantenna and the QE. The system is illuminated by a plane wave propagating along the $z$-axis with electric field polarized along the $x$-axis. (b) and (c) Extinction cross-section of the hybrid system, $\sigma_{\mathrm{Ext}}$, normalized to the spectra of the bare sphere, $\sigma_{\mathrm{Ext}}^{(0)}$ as obtained within (b) the simple dipole-dipole interaction model described in sections 2 and 3.3.1 and (c) within the rigorous Mie's theory calculations. The spectra are vertically displaced by 1.25 for clarity and plotted as a function of the wavelength detuning ($\Delta\lambda = \lambda - \lambda_0$) with respect to the resonance of both nanoantenna and QE ($\lambda_0$). Each spectral line is evaluated for different distances, $d$, between the QE and the surface of the antenna (indicated in the figure). In both calculations, the radius of the silver spherical nanoparticle is $r = 20$ nm. The exact calculations consider the experimental permittivity of silver [36] to model the response of the nanoantenna (leading to $\lambda_0 = 359.78$ nm). On the other hand, in the approximated dipole-dipole interaction model we use the Drude model to describe the dielectric function of the silver nanoantenna, $\varepsilon_{\mathrm{a}} = 1 - \omega_{\mathrm{p}}^2/[\omega(\omega + i\kappa)]$, with $\hbar\omega_{\mathrm{p}} = 6.06$ eV and $\hbar\kappa = 0.62$ eV, obtaining $\lambda_0 = 354.59$ nm for the dipolar excitation.

$$\alpha_{\mathrm{a}} = \frac{A_{\mathrm{a}}}{\omega_R^2 - \omega^2 - i\kappa\omega}, \tag{4}$$

where the strength of the coupling between the two dipoles is determined by the polarizability amplitude of the QE, $A_{\mathrm{e}}$, and that of the plasmonic nanoantenna $A_{\mathrm{a}}$. The frequency $\omega_R = \omega_p/\sqrt{3}$ is the frequency of the dipolar plasmon resonance in the nanoantenna (with $\omega_p$ the Drude plasma frequency). Here we chose $\omega_R$ to match $\omega_0$ ($\omega_R = \omega_0$), the resonant excitation frequency of the QE. Last, $\omega = 2\pi c_0/\lambda$ is the frequency (with $\lambda$ the wavelength) and $\gamma$ and $\kappa$ are the spontaneous decay rate of the QE and the plasmonic intrinsic decay rate, respectively. Throughout this work we consider that the dipole moment of the excitonic transition is $\mu = 0.05e{\cdot}$nm ($e$ is the electron charge), which sets the polarizability amplitude of the QE $A_{\mathrm{e}} = 2\omega_0\mu^2/\hbar$ and the spontaneous decay rate $\gamma = \omega_0^3\mu^2/(3\pi\varepsilon_0\hbar c_0^3)$ ($\hbar$ is the reduced Planck constant). We do not consider other intrinsic molecular losses beyond $\gamma$. Substituting Eqs. (3) and (4) into Eqs. (1) and (2) one obtains:

$$(\omega_0^2 - \omega^2)p_{\mathrm{e}} - i\omega\gamma p_{\mathrm{e}} = A_{\mathrm{e}}G_{x,x}^{\mathrm{qs}}p_{\mathrm{a}}, \tag{5}$$

$$(\omega_0^2 - \omega^2)p_{\mathrm{a}} - i\omega\kappa p_{\mathrm{a}} = A_{\mathrm{a}}G_{x,x}^{\mathrm{qs}}p_{\mathrm{e}} + A_{\mathrm{a}}E_0. \tag{6}$$

Optics EXPRESS

Here, the polarizability amplitude of the nanoantenna determines how efficiently is the system excited (via the term $A_a E_0$). Equations (1)–(6) and the expression used to obtain $A_a$ are discussed in more detail in section 3.3.1.

We note that Eqs. (5) and (6) are very similar to those obtained with phenomenological models that assume that the QE and the plasmonic nanoparticle can be treated as two coupled harmonic oscillators. This coupled-harmonic-oscillators model has been frequently used to describe the interaction between quantum emitters and nanoantennas [14,37,38].

We show in Fig. 1(b) the extinction cross-section spectrum of the hybrid QE-nanoantenna system obtained using Eqs. (5) and (6) for different values of the separation distance $d$ between the QE and the surface of the nanoantenna (the value of $d$ affects the quasistatic Green's function, $G^{qs}_{x,x}$, and, thus, the QE-nanoantenna interaction). The extinction cross section $\sigma_{Ext}$ is normalized to the corresponding value of the bare nanoantenna $\sigma^{(0)}_{Ext}$ and it is obtained assuming that the direct emission of the QE is negligible ($p_a \gg p_e$), which is a typical situation in plasmonic systems. In this case, the optical theorem [39] gives

$$\sigma^{simp}_{Ext}(\omega) = \frac{2\pi}{\lambda \varepsilon_0} \mathrm{Im}\left\{\frac{p_a(\omega)}{E_0}\right\}, \tag{7}$$

where $\varepsilon_0$ is the vacuum permittivity and the super index "simp" emphasizes that this is a simplified expression that only considers the emission from the nanoantenna.

The normalized extinction cross-section in Fig. 1(b) features an almost constant background and the emergence of a spectrally narrow dip at the resonant wavelength $\lambda_0$ for all the separation distances $d$ considered. The background corresponds to the very broad plasmonic response and the dip to the Fano feature. Importantly, the Fano dip obtained within this simple dipole-dipole interaction model (Eqs. (5)–(7)) is always perfectly symmetric. The origin of this symmetric Fano dip can also be understood from a different perspective as a result of the interference of the fields scattered by the systems (see Appendix A).

We next use Mie's theory to obtain the exact electromagnetic response of the system (Supplement 1). Figure 1(c) shows the resulting extinction cross section obtained for the same system and distances $d$ as in Fig. 1(b). These exact calculations exhibit again a broad background due to the response of the bare plasmonic nanoantenna and a narrow Fano feature caused by the coupling between the QE exciton and the plasmonic resonance of the nanoantenna. However, the Fano lineshapes show clear differences compared to those obtained with the simple dipole-dipole interaction model (Eqs. (5)–(7) and Fig. 1(b)). Overall, the Fano features are broader for the exact calculations than for the simple model. Further, the exact calculation also results in a shift of the Fano features, induced by the photonic Lamb shift, not included in the simple model. The shift and larger broadening are clearer for small nanoantenna-QE separation distances ($d$<20 nm) and are mainly a consequence of the coupling between the QE exciton and the higher-order modes of the nanoantenna [40–51]. Crucially, the Fano feature obtained within the exact calculations is not necessarily a perfectly symmetric dip, but it can take different lineshapes. This shape evolves from a broad and almost symmetric dip at short separation distances ($d$<15 nm) towards a narrow and almost symmetric peak at large separation distances ($d$>60 nm). In the range between these two extremes, the Fano feature becomes clearly asymmetric.

Thus, we have shown that the prediction of a symmetric Fano dip obtained with a simple dipole-dipole interaction model can strongly differ from the results of the exact calculations, where significantly asymmetric lineshapes emerge (see also discussion based on fields interference in appendix A). We emphasize that this asymmetry is not due to plasmon-exciton detuning as the resonance condition of zero detuning is preserved in all cases. In the following, we analyze in detail the different physical mechanisms that lead to asymmetric Fano lineshapes for QE-nanoantenna systems under resonant conditions.

Optics EXPRESS

## 3. Dissection of the asymmetry

To analyze the Fano asymmetry in more detail we first describe, in subsection 3.1, an equation of the Fano lineshape that allows for quantifying the asymmetry with a single factor $q$ [14,26]. Then, in subsection 3.2, we show that this asymmetry factor can be decomposed into two contributions, each of them described by a simple analytical expression. We finally evaluate in subsection 3.3 the asymmetry factor using a series of analytical dipole-dipole interaction models of increasing accuracy to understand how different phenomena affect the Fano profile. Throughout this section we study the same system introduced in section 2 (scheme in Fig. 1(a)).

### 3.1. Fano lineshape

The extinction cross-section of a QE-nanoantenna system excited by a plane wave can be described by a modified Fano lineshape [14,26] (assuming that the spectral width of the QE emission is much smaller than the width of the spectral response of the nanoantenna):

$$\frac{\sigma_{\mathrm{Ext}}(\Omega)}{\sigma_{\mathrm{Ext}}^{(0)}} \approx \frac{(\Omega+q)^2+B}{\Omega^2+1}, \tag{8}$$

which depends on three parameters, $q$, $\Omega$, and $B$ (see section S1 of Supplement 1 for a detailed derivation). $q$ is the total asymmetry factor (also called Fano-parameter) that captures the asymmetry of the Fano lineshape of the extinction cross-section spectrum, and it is the main focus of this work (in section S6 of Supplement 1 we also study the asymmetry of the Fano features found in resonant conditions in the scattering cross-section spectrum). $\Omega$ is a normalized frequency given by

$$\Omega = \frac{\omega_0'^2 - \omega^2}{\omega\gamma'}, \tag{9}$$

where

$$\omega_0' = \omega_0 + \Delta\omega, \tag{10}$$

and

$$\gamma' = (1+P_{\mathrm{F}})\gamma. \tag{11}$$

$\Delta\omega$ is the photonic Lamb Shift that corresponds to a slight shift in the resonant frequency from $\omega_0$ to $\omega_0'$. $P_{\mathrm{F}}$ in Eq. (11) denotes the Purcell Factor, which describes the broadening of the dip and which is directly related to an increase of the local photonic density of states [40]. Both effects can be clearly observed in the spectra of Fig. 1(c). The expression of $\gamma'$ assumes no intrinsic losses beyond $\gamma$, but it can be modified in a straightforward manner to include additional intrinsic losses. Last, $B$ in Eq. (8) is the zero-dip parameter that can be related to the factor $q$ and the contrast $C = \sqrt{2(B+1)q^2 + (B-1)^2 + q^4}$. Here, we define the contrast $C$ of the Fano feature as the difference between the maximum and the minimum of the Fano feature in the normalized extinction cross-section spectrum (see inset in panel 2 of Fig. 2(e)).

Thus, changes on the Fano spectral lineshape can be understood by analyzing the parameters, $q$, $C$, $P_{\mathrm{F}}$, and $\Delta\omega$ (the last two determining $\Omega$). These parameters can be obtained from the classical Green's function and the field enhancement of the plasmonic antenna at the position of the emitter according to the expressions derived in Supplement 1, section S1. In Fig. 2(a)-(d), we systematically study the dependence of these parameters with the radius of the silver spherical nanoparticle, $r$, and the distance between the antenna and the emitter, $d$. All values are obtained from exact Mie's theory calculations using the experimental values of the silver permittivity [36] and assuming resonant conditions; *i.e.*, for each radius, we find the frequency of the dipolar plasmonic resonance of the antenna (lowest-energy peak in the extinction cross-section spectrum of the bare nanoantenna), and we modify the energy of the QE transition accordingly. To illustrate

Optics EXPRESS

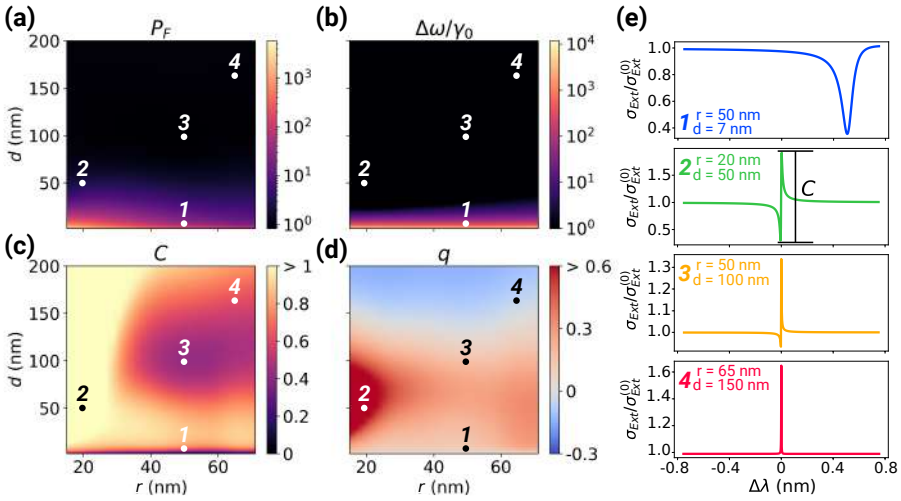


**Fig. 2.** (a-d) Contour plots of the parameters defining the Fano lineshape, obtained within Mie's theory. (a) Purcell Factor, $P_F$, (b) Lamb Shift, $\Delta\omega$, (c) contrast, $C$, and (d) total asymmetry factor, $q$ as a function of the distance, $d$ (the minimum distance in the panels is $d = 2$ nm), from the QE to the surface of a silver spherical antenna with different radius, $r$. The resonance of the QE is chosen to match the frequency of resonance of the nanoantenna for all sizes of particles, $r$. (e) Normalized extinction spectra evaluated for points marked as 1, 2, 3, and 4 in (a)-(d). The values of $r$ and $d$ for each point are indicated in the labels of (e).

the resulting Fano lineshape described by the parameters in Figs. 2(a)-(b), we also show, in Fig. 2(e), the extinction cross section spectrum for four different points indicated in Figs. 2(a)-(d) (the values of $r$ and $d$ for each point are given in the labels of Fig. 2(e)).

For all the radii considered, the Purcell Factor, $P_F$, (Fig. 2(a)), and the photonic Lamb shift $\Delta\omega$ (Fig. 2(b)) strongly increase when the QE approaches the antenna, as shown in previous studies [40–48]. This increase is due to the more efficient coupling of the QE with the plasmonic modes of the nanoantenna, particularly with high-order modes. In subsection S7 of Supplement 1, we show a cut in the contour plot of $P_F$ in Fig. 2(a) as a function of the separation distance $d$ for three fixed reference values, $r = 15$ nm, $r = 45$ nm, and $r = 65$ nm.

On the other hand, the contrast, $C$, presents a more complex dependence with the radius, $r$, and the distance, $d$ (Fig. 2(c)). We can distinguish three different distance regimes in this figure. For short distances ($d \lesssim 10$ nm), the QE couples very efficiently to the higher-order modes of the spherical nanoparticle, and the resulting quenching of the emission [49–51] leads to the disappearance of the Fano dip (small contrast). For intermediate distances (compared to the radius, *i.e.* 10 nm $\lesssim d \lesssim 3r$), the quenching becomes less significant, and the Fano feature emerges with a reasonably big contrast ($1 \gtrsim C \gtrsim 0.5$, purple-reddish region in Fig. 2(c)). In this regime of distances, the contrast is smaller for spheres with $r \gtrsim 40$ nm, which is mainly a consequence of two destructive interference effects, the first between the excitation of the QE by the illumination plane–wave and by the antenna-induced near fields, and the second between the light emitted by the QE directly and via the nanoantenna. Last, as the separation distance is made significantly larger than the radius ($d \gtrsim 3r$), the QE progressively decouples from the nanoantenna, and the extinction cross-section of the whole system evolves toward the superposition of the peak of the extinction cross-section of the QE in a vacuum on top of the broad background spectrum of the bare spherical nanoparticle. We can then express the extinction cross–section of the whole system at very long separation distances as $(\sigma^{(0)}_{\text{Ext}} + \sigma^{\text{QE}}_{\text{Ext}})/\sigma^{(0)}_{\text{Ext}}$, where $\sigma^{\text{QE}}_{\text{Ext}}$ is the extinction cross-section of the QE in a vacuum. As we have considered that the

Optics EXPRESS

QE only has radiative losses due to the spontaneous decay, $\sigma_{\mathrm{Ext}}^{\mathrm{QE}}$ is larger than the extinction cross-section of the bare spherical nanoparticle $\sigma_{\mathrm{Ext}}^{(0)}$ [52] ($\sigma_{\mathrm{Ext}}^{\mathrm{QE}} = 6\pi(\omega_0/c_0)^2 > \sigma_{\mathrm{Ext}}^{(0)}$), and the contrast becomes higher than one, $C>1$.

Last, Fig. 2(d) shows the relatively complex dependence of the total asymmetry factor $q$ with radius $r$ and distance $d$. The Fano asymmetry is small ($|q|<0.2$) for $d \lesssim 10$ nm (corresponding to a symmetric dip) and for large distances, $d \gtrsim 150$ nm, (corresponding to an almost symmetric peak). At intermediate distances (10 nm $\lesssim d \lesssim$ 150 nm) the asymmetry is significantly larger, with a maximum value at a distance $d \sim 50$ nm, which is strongly dependent on the radius. We also find that at large distances ($d \gtrsim 150$ nm) the asymmetry can take negative values and show a damped oscillatory behavior of $q$ with $d$ (the dependence of $q$ for a larger range of distances is shown in section S5 of Supplement 1). Understanding this complex behavior is the main objective of this work and it is analyzed in detail next.

### 3.2. Analytical expression of the total asymmetry factor

To further analyze the total asymmetry factor $q$ of the Fano lineshape, we first separate it into two main contributions, $q_{\mathrm{E}}$ and $q_{\mathrm{R}}$ according to the following analytical expression (derived in section S1 of Supplement 1 by applying the optical theorem [39]):

$$q = \frac{A_{\mathrm{e}}\lambda_0^2}{2\pi\sigma_{\mathrm{Ext}}^{(0)}\gamma' c_0}\mathrm{Re}\{(-iz_{\mathrm{d}})e^{-i2\pi z_{\mathrm{d}}/\lambda_0}(K+1)G_{x,x}^{\mathrm{FF}}\} = \\ = \underbrace{\left(\frac{A_{\mathrm{e}}}{2\sigma_{\mathrm{Ext}}^{(0)}c_0\varepsilon_0}\frac{\mathrm{Im}\{K\}}{\gamma'}\right)}_{q_{\mathrm{E}}} + \underbrace{\left(\frac{A_{\mathrm{e}}}{2\sigma_{\mathrm{Ext}}^{(0)}c_0\varepsilon_0}\frac{\mathrm{Re}\{K\}\mathrm{Im}\{K\}}{\gamma'}\right)}_{q_{\mathrm{R}}}, \tag{12}$$

where $\varepsilon_0$ is the vacuum permittivity, $\gamma'$ corresponds to the effective decay rate of the QE (including the Purcell effect induced by the nanoantenna, Eq. (11)), $A_{\mathrm{e}}$ is the amplitude of the polarizability of the QE (Eq. (3)), and $\sigma_{\mathrm{Ext}}^{(0)}$ is the extinction cross section of the nanoantenna in the absence of the QE. $G_{x,x}^{\mathrm{FF}}$ is the $(x,x)$ component of the Green's tensor that gives the total emission of the QE towards a detector situated in the far field in the forward $z$ direction (considering the direct emission as well as the antenna-mediated one), and $z_{\mathrm{d}}$ is the distance to the detector (which does not affect the final result). $K$ is the field enhancement factor that we define as $E_x^{\mathrm{AE}} = KE_0$, where $E_x^{\mathrm{AE}}$ is the x-component of the electric field induced by the nanoantenna at the position of the emitter under illumination by a plane wave of amplitude $E_0$. $K$ does not include the direct illumination of the emitter.

The first line in Eq. (12) shows the dependence of the total asymmetry factor $q$ on the emission and the excitation of the QE, *i.e.* on $G_{x,x}^{\mathrm{FF}}$ and $(K+1)$ respectively. Further, we can relate the emission and the excitation of the QE using reciprocity [53–55], and write $q$ only as a function of the enhancement $K$ (second line of Eq. (12), see section S1 of Supplement 1). This simplification allows us to focus on the effect of the enhancement $K$, and to split $q$ into two different contributions that we denote $q_{\mathrm{R}}$ and $q_{\mathrm{E}}$ (as indicated in Eq. (12)).

We focus first on the asymmetry factor $q_{\mathrm{R}}$. In section S2 of Supplement 1, we show that this factor fully describes the asymmetry in resonant conditions if we ignore the direct excitation and emission of the QE ($q = q_{\mathrm{R}}$). If we decompose explicitly the field enhancement into its amplitude $|K|$ and phase $\varphi_{\mathrm{A}}$, we obtain:

$$q_{\mathrm{R}} = \frac{A_{\mathrm{e}}}{2\sigma_{\mathrm{Ext}}^{(0)}c_0\varepsilon_0}\frac{|K|^2\sin(2\varphi_{\mathrm{A}})}{\gamma'}. \tag{13}$$

Optics EXPRESS

We can further simplify Eq. (13) by connecting $|K|$ with the enhanced decay rate $\gamma'$ as:

$$\frac{|K+1|^2}{\gamma'} = \frac{\eta}{D\gamma}, \tag{14}$$

where $\eta$ is the radiative yield (defined as the ratio between the radiative and the total decay rate of the QE in the presence of the nanoantenna) [49]. $D$ is a parameter that models the change of the directionality of the emission of the QE due to the presence of the nanoantenna [44,56] and it is typically close to one ($D \sim 1$). We show in the section S3 of Supplement 1 how to derive Eq. (14) by using reciprocity [53–55] and provide the exact definition of the directionality $D$. For plasmonic nanostructures $|K|$ is often much larger than 1 and we can then approximate the equality in Eq. (14) as $\frac{|K|^2}{\gamma'} \approx \frac{\eta}{D\gamma}$, which results in

$$q_R \approx \frac{A_e}{2\sigma_{Ext}^{(0)} c_0 \varepsilon_0} \frac{\eta}{D\gamma} \sin(2\varphi_A). \tag{15}$$

Thus, the asymmetry factor $q_R$ only depends in this case on the phase of the field enhancement $\varphi_A$, but not on its amplitude. In the simplified dipole-dipole interaction model considered in section 2 (Eqs. (5)–(7)), $\varphi_A = \pi/2$ at resonance, and thus $q_R = 0$. When $\varphi_A$ deviates from $\pi/2$ (for example, due to retardation) $q_R \neq 0$, introducing an asymmetry in the Fano feature.

Figure 3(a) shows the values of $q_R$ calculated using the full electromagnetic Mie's theory to describe the scattering of the silver spherical nanoparticle. $q_R$ is again plotted in resonant conditions as a function of the radius of the silver spherical nanoparticle $r$ and the distance $d$ between the emitter and the surface of the nanoparticle. $|q_R|$ is largest for intermediate distances (20 nm $\lesssim d \lesssim$ 80 nm) where retardation is significant (and thus $\varphi_A$ substantially different than $\pi/2$) and $|K|$ is of the order of 1 (see Eq. (13)). At shorter distances, $|K|$ increases so that Eq. (15) becomes more accurate, and at the same time $\sin(2\varphi_A)$ takes values close to 0, since retardation becomes negligible. As a consequence, $|q_R|$ strongly decreases. On the other hand, at larger distances, $|K|^2$ becomes very small and $\gamma'$ becomes similar to the intrinsic decay rate $\gamma$. Thus, $|q_R|$ gradually approaches 0, according to Eq. (13).

We next analyze the second asymmetry contribution, $q_E \propto \mathrm{Im}\{K\}/\gamma'$ (Eq. (12)), which appears when the direct excitation and emission of the QE is considered. The results of the Mie's calculation of $q_E$ are shown in Fig. 3(b). $q_E$ is small for long QE–nanoantenna distances

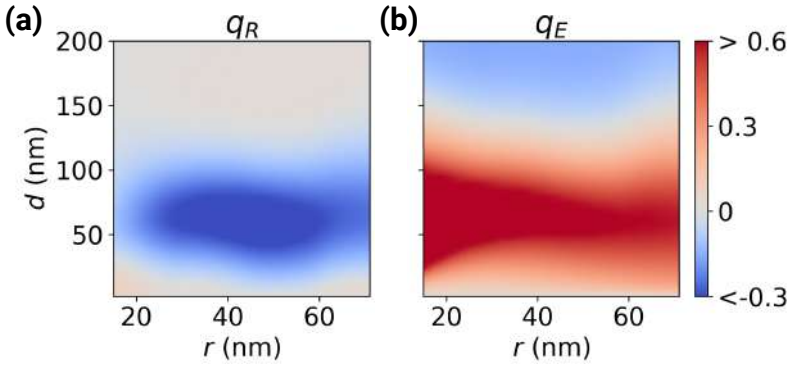


**Fig. 3.** Values of the two asymmetry factors $q_R$ and $q_E$. The values of (a) $q_R$ and (b) $q_E$ given in Eq. (12) are shown for different radius $r$ and distances of the QE to the surface $d$ (the minimum distance in the panels is 2 nm). These results are obtained using Mie's theory and the experimental permittivity of silver [36]. For each radius, $r$, the resonance of the QE is chosen to match the frequency of the resonance of the nanoantenna.

Optics EXPRESS

($d$>100 nm) because $|K|$ approaches 0 and $\gamma' \approx \gamma$ (we focus here on the absolute value of $q_E$ and we discuss the change of sign for $d \approx 150$ nm below). Indeed, for long distances the system starts to decouple and we can approximately consider the response of the QE and the nanoantenna separately. These two contributions interfere constructively so that we can directly add up their respective extinction cross sections according to the optical theorem (see section S1 of Supplement 1). Thus, the final extinction cross-section spectrum is given by a symmetric peak due to the QE emission added to the broad plasmonic peak (panel 4 in Fig. 2(e)), corresponding to low values of $q_E$ and $q$.

Furthermore $q_E$ is also small at short distances ($d \lesssim 20$ nm). In this case $|K| \gg 1$ so that $q_E \propto \mathrm{Im}\{K\}/\gamma' \to 0$ because $\gamma' \propto |K+1|^2\gamma$ (from Eq. (14)). These low values of $q_E$ for small $d$ could be expected since $q_E$ is given by the direct excitation of the QE; therefore $q_E$ becomes negligible if the direct excitation is very small in comparison with the excitation via the nanoantenna.

$q_E$ thus becomes largest for intermediate separation distances (20 nm $\lesssim d \lesssim$ 80 nm), as Fig. 3(b) shows. In this range of distances, the field induced by the spherical nanoparticle is of similar strength as the field of the incident plane-wave ($|K| \approx 1$). The excitation of the QE is then given by an interplay between the direct and the antenna-mediated illumination, which carry a different phase leading to large values of the asymmetry factor $q_E \gtrsim 0.6$. We note that in all this discussion, we have focused on the direct excitation, but a similar analysis can also be developed in terms of the direct emission of the antenna, according to reciprocity, which was adopted in the derivation of the expression of $q_E$ in Eq. (12). The analysis of the $q_E$ and $q_R$ factors thus already gives insights into the general behavior of the total asymmetry factor $q$ (Eq. (12)) shown in Fig. 2(d). Notably, the relatively low values of $q$ obtained for intermediate radius (40 nm $\lesssim r \lesssim$ 60 nm) in the 20 nm $\lesssim d \lesssim$ 80 nm separation distance range, which results in a characteristic "saddle" shape, are due to the addition of two asymmetry factors, $q = q_E + q_R$ of similar absolute value but opposite sign.

### 3.3. *Effect of different optical response approximations on the asymmetry*

To further understand the origin of the asymmetry $q$ and its contributions, $q_E$ and $q_R$, under resonant conditions, we adopt different analytical dipole-dipole interaction models of increasing levels of complexity. A general dipole-dipole description of the QE-nanoantenna system introduced in section 2 (Fig. 1) is given by

$$p_e = \alpha_e(E_0 + G_{x,x}p_a), \tag{16}$$

$$p_a = \alpha_a(E_0 + G_{x,x}p_e), \tag{17}$$

where $E_0$ is the amplitude of the excitation field and $p_a$ and $\alpha_a$ are the induced dipole and the polarizability of a single plasmonic mode of the nanoantenna (in our case the dipolar plasmonic mode), respectively. $p_e$ and $\alpha_e$ are the corresponding magnitudes of the exciton of the QE. $\alpha_e$ is given by Eq. (3) and during this section we use different models to describe $\alpha_a$. $G_{x,x}$ is the $\{x,x\}$-component of the Green's function that describes the interaction between the QE and the nanoantenna (either the quasistatic or the fully retarded expression).

Finally, the extinction cross section of the QE-nanoantenna system can be obtained from the optical theorem [39] as:

$$\sigma_{\mathrm{Ext}} = \frac{2\pi}{\lambda\varepsilon_0}\mathrm{Im}\left\{\frac{p_a + p_e}{E_0}\right\}. \tag{18}$$

In the following, we introduce different approximations in Eqs. (16)–(18). In subsection 3.3.1 we first discuss the simplifications necessary to reproduce the simple model discussed in section 2 (Eqs. (1)–(6)). We then systematically modify this model to progressively build up a more rigorous model that nicely reproduces results obtained with Mie's theory (Figs. 2(d) and 3). In

Optics EXPRESS

this manner we can better identify how different effects contribute to each of the features of the total asymmetry factor in resonance.

We show in Fig. 4(a)-(g) the total asymmetry factor $q$ and its contributions $q_R$ and $q_E$ when different modifications of the dipole-dipole interaction models are implemented. Each column of the figure shows the results for particular assumptions in the model (as indicated by labels at the bottom) and the first, second, and third row of the figure provide the values of $q_R$, $q_E$, and $q$ (respectively) evaluated for the same ranges of radius $r$ and distances $d$ as those in Figs. 3 and 2(a)-(d).

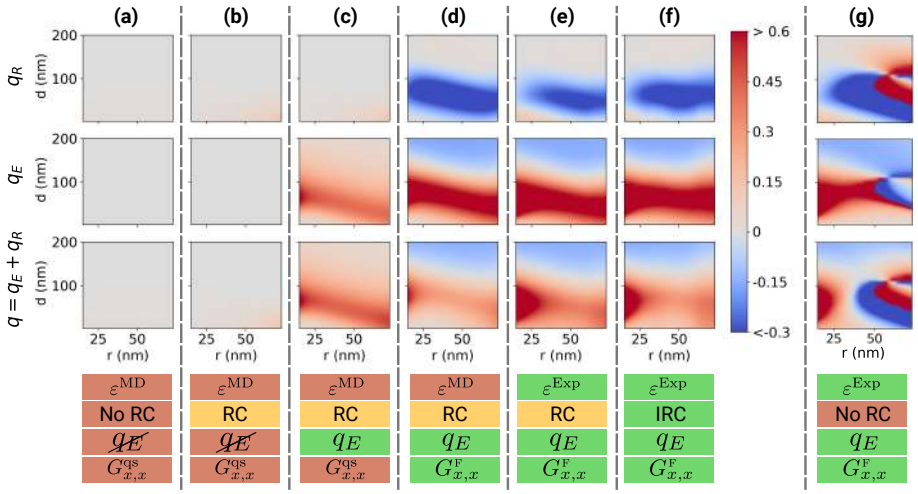


**Fig. 4.** Behavior of the asymmetry factors in the extinction cross-section in resonant conditions (zero detuning between the nanoantenna and QE resonances) according to different models. Each (a)-(g) column contains three panels showing the values of the asymmetry factors $q_R$ (first row), $q_E$ (second row), and the total asymmetry factor, $q = q_E + q_R$, (third row). The asymmetry factors are calculated for different values of the radius $r$ of the silver spherical nanoantenna, and the distance $d$ between the nanoantenna and the QE. The resonance of the QE is chosen to match the frequency of the dipolar resonance of the nanoantenna for each radius $r$. The values shown in each (a)-(g) column are obtained using the different models described in subsection 3.3. The values of the asymmetry factors are saturated for values larger than 0.6 and smaller than −0.3. At the bottom of each (a)-(g) column, we indicate the main features of the considered model with four labels colored in green, yellow, or red. The red labels indicate a less accurate description of a given feature, while the yellow and green indicate a progressively more accurate description. The label "$\varepsilon^{MD}$" indicates that we use the modified Drude expression to describe the permittivity of the nanoantenna. "$\varepsilon^{Exp}$" indicates that we use the experimental values of the permittivity of the nanoantenna [36]. "No RC" indicates that we do not consider the radiative correction. "RC" indicates that we consider a simple radiative correction. "IRC" indicates that we use an improved version of the radiative correction (31) [57]. "$q_E$" indicates that we do not consider the direct excitation and emission of the QE (and thus $q_E = 0$). "$q_E$" indicates that we do consider the direct and emission of the QE. "$G^{qs}_{x,x}$" indicates that we use the quasistatic Green's function described in section 2. "$G^{F}_{x,x}$" indicates that we use the full expression of the Green's function [40].

Optics EXPRESS

#### 3.3.1. Simple reference model

We consider first the simple dipole-dipole interaction model introduced in section 2. (Eqs. (5)–(7)). This simple model describes the optical response of the coupled QE-nanoantenna system using four simplifications in Eqs. (16)–(18):

i) The polarizability of the spherical nanoantenna, $\alpha_a$, is obtained using the quasistatic approximation,

$$\alpha_a = 4\pi\varepsilon_0 r^3 \frac{\varepsilon_a - 1}{\varepsilon_a + 2}, \tag{19}$$

where $\varepsilon_a$ is the dielectric permittivity of the nanoantenna.

ii) We describe the permittivity of the metallic nanoantenna using the Drude's model, $\varepsilon_a = 1 - \omega_p^2/[\omega(\omega + i\kappa)]$, where $\omega_p$ is the plasma frequency, and $\kappa$ are the plasmon losses. Inserting $\varepsilon_a$ into Eq. (19), directly recovers the expression of the polarizability given in Eq. (4), with $A_a = 4\pi\omega_p^2\varepsilon_0 r^3/3$ and $\omega_0 = \omega_p/\sqrt{3}$. This expression of $\alpha_a$ is purely imaginary at resonance ($\omega = \omega_0$).

iii) The QE is only excited by the field created by the nanoantenna (corresponding to $G_{x,x}p_a$ in Eq. (16)), neglecting the direct excitation of the QE by the incident plane wave. Further, we also neglect the direct emission of the QE to the far field as it is usually smaller than the emission mediated by the nanoantenna. According to the optical theorem, the extinction cross-section is then directly given by the induced dipole at the nanoantenna, $\sigma_{Ext} \propto \mathrm{Im}\{p_a\}$.

iv) The interaction between the QE and the nanoantenna is described using the quasistatic Green's function

$$G_{x,x}^{qs} = \frac{1}{2\pi\varepsilon_0(r+d)^3}, \tag{20}$$

which is real-valued.

In the following, it is useful to summarize the optical response of the QE-nanoantenna system assumed in this simple model by displaying the set of equations summarizing the model:

$$p_a = \alpha_a(E_0 + G_{x,x}^{qs} p_e), \tag{21}$$

$$p_e = \alpha_e K E_0, \tag{22}$$

$$KE_0 = G_{x,x}^{qs} p_a, \tag{23}$$

$$\gamma' = \left[1 + \mathrm{Im}\left\{\frac{A_e\alpha_a}{\gamma\omega_0}(G_{x,x}^{qs})^2\right\}\right]\gamma, \tag{24}$$

$$\sigma_{Ext} = \frac{2\pi}{\lambda\varepsilon_0}\mathrm{Im}\left\{\frac{p_a}{E_0}\right\}, \tag{25}$$

where we have introduced the connection of the field enhancement factor $K$ at the position of the QE with the induced dipole moment of the nanoantenna and the Green's function (Eq. (23)). We also include the expression of the Purcell-enhanced effective decay rate of the QE, $\gamma'$ (Eq. (24)). Both $K$ and $\gamma'$ are key parameters to understand the changes on the asymmetry of the Fano feature. This simple reference model always predicts a zero asymmetry factor ($q = 0$, $q_E = 0$, and $q_R = 0$), as shown in section 2, and thus it is not included in Fig. 4.

Optics EXPRESS

#### 3.3.2. Contribution of $d$-electrons to the permittivity

The first modification to the simple dipole-dipole interaction model consists in changing the dielectric permittivity of the nanoantenna from the simple Drude model $\varepsilon_a = 1 - \omega_p^2/[\omega(\omega + i\kappa)]$ into a modified Drude expression $\varepsilon_a^{MD} = \varepsilon_\infty - \omega_p^2/[\omega(\omega + i\kappa)]$ (with $\varepsilon_\infty = 6$, $\hbar\omega_p = 9.17$ eV, and $\hbar\kappa = 21$ meV). $\varepsilon_a^{MD}$ approximately includes the effect of the $d$-electrons of silver, which allows for better describing the optical response of the silver nanoantenna. Within this description, Eqs. (21)–(25) remain valid except that the polarizability of the nanoantenna is now $\alpha_a^{MD} = 4\pi r^3(\varepsilon_a^{MD} - 1)/(\varepsilon_a^{MD} + 2)$, so that $\alpha_a^{MD}$ is no longer a perfect Lorentzian function. As a consequence the induced field enhancement $K$ is not purely imaginary at resonance and the Fano feature at resonance is no longer perfectly symmetric, $q = q_R \neq 0$, according to Eq. (15) ($q_E = 0$ because we are not considering yet the contribution of the direct emission and excitation of the QE). We show in Fig. 4(a) the results of the total asymmetry factor $q$ and its contributions $q_E$ and $q_R$ obtained within this model as a function of the radius $r$ of the spherical nanoparticle and the distance $d$ between the QE and the surface of the nanoparticle. We observe how, although within this model $q \neq 0$ and $q_R \neq 0$, the asymmetry remains very small with $q \leq 0.01$.

#### 3.3.3. Simple radiative correction

We next consider a simple radiative correction to the nanoantenna polarizability $\alpha_a^{RC} = \alpha_a^{MD}/[1 - i\alpha_a^{MD}(2\pi/\lambda)^3/(6\pi\varepsilon_0)]$ [40,57,58] that accounts for the radiation damping of the nanoantenna in a vacuum. This correction incorporates the scattering losses that broaden the resonance, which were neglected in the previous quasistatic description (Fig. 4(a)). We note that, once the radiative correction is introduced, the maximum of the extinction cross section $\sigma_{Ext}^{(0)}$ of the bare nanoantenna dipolar resonance red-shifts spectrally with increasing size, and is found at a slightly shorter wavelength than the corresponding maximum of the near–field enhancement $|K|$ [59,60]. In this paper we always consider that the resonant frequency of the QE, $\omega_0$, matches the frequency at which $\sigma_{Ext}^{(0)}$ is maximum. We show in section S5 of Supplement 1 that the effect of setting $\omega_0$ to the maximum of $|K|$ is weak.

We show in Fig. 4(b) (second column of the figure) the resulting total asymmetry factor $q$ (and its contributions, $q_E$ and $q_R$) obtained after substituting $\alpha_a^{MD}$ by $\alpha_a^{RC}$ in the simplest dipole-dipole interaction model (21–23). This change mainly affects the value of $K$, which acquires a larger real part at resonance as compared to the previous model (the phase of $K$ deviates further from $\pi/2$) and, thus, $q = q_R$ increases (Eq. (13)), with $q_E$ remaining equal to zero. In particular, $q_R$ becomes larger with increasing $r$, as the effect of the radiative correction increases with the size of the nanoantenna. $q_R$ also increases for shorter $d$ due to the stronger enhancement $|K|$. However, the asymmetry remains small (hardly noticeable in Fig. 4(b), with $\max(q_R) \approx 0.14$). Last, we note that this low value of $q$ may lead to think that the radiative correction is of little importance in the description of the total asymmetry factor. However, we emphasize in subsection 3.3.7 that, once we go beyond the quasistatic approximation of the Green's function, it is critical to consider a correct description of the radiative correction.

#### 3.3.4. Direct excitation and emission of the QE

In the next step we introduce the direct excitation of the QE by the plane wave and the direct emission of the QE to the far field (third column, Fig. 4(c)). These two effects are introduced at the same time because, due to reciprocity [53–55], their contribution to the asymmetry is identical (demonstration in section S1 of Supplement 1). After all these changes the response of the system is given by the following modified equations:

$$p_a = \alpha_a^{RC}(E_0 + G_{x,x}^{qs} p_e), \tag{26}$$

$$p_e = \alpha_e(1 + K)E_0, \tag{27}$$

Optics EXPRESS

$$KE_0 = G^{\mathrm{qs}}_{x,x} p_{\mathrm{a}}, \tag{28}$$

$$\gamma' = \left[1 + \mathrm{Im}\left\{\frac{A_{\mathrm{e}}\alpha_{\mathrm{a}}^{\mathrm{RC}}}{\gamma\omega_0}(G^{\mathrm{qs}}_{x,x})^2\right\}\right]\gamma, \tag{29}$$

$$\sigma_{\mathrm{Ext}} = \frac{2\pi}{\lambda\varepsilon_0}\mathrm{Im}\left\{\frac{p_{\mathrm{a}} + p_{\mathrm{e}}}{E_0}\right\}. \tag{30}$$

The direct excitation of the QE by the incident plane wave of amplitude $E_0$ is described by the term $\alpha_{\mathrm{e}}E_0$ in Eq. (27). Similarly, the direct contribution from the QE to the extinction cross section is given by the term $\propto \mathrm{Im}\{p_{\mathrm{e}}\}$ in Eq. (30). In this scenario, the $q_{\mathrm{E}}$ contribution to the asymmetry is no longer zero, and the full expression of the total asymmetry factor, $q = q_{\mathrm{E}} + q_{\mathrm{R}}$, needs to be considered (Eq. (12)). On the other hand, $q_{\mathrm{R}}$ remains unchanged as compared to the previous model.

As shown in Fig. 4(c) the resulting $q_{\mathrm{E}}$ dominates the total asymmetry factor $q$, and follows similar trends with distance as those described when discussing the results of the exact calculation in Fig. 3. $q_{\mathrm{E}}$ is small at long separation distances ($d$>100 nm) because the QE and the nanoantenna start to behave independently, and also at short distances ($d \lesssim 20$ nm) because the direct excitation of the QE is very small compared to the excitation via the nanoantenna. $q_{\mathrm{E}}$ is thus maximum at intermediate distances within this model (20 nm $\lesssim d \lesssim$ 80 nm) where the excitation of the QE via the nanoantenna is of the same order of magnitude than the direct excitation by the incident plane wave. The distance that maximizes $q_{\mathrm{E}}$ follows a linear dependence with increasing radius $r$. More precisely, the maxima are found for an approximately constant distance between the QE and the center of the nanoantenna ($d + r$). This behavior occurs because in this description the near fields are evaluated using the quasistatic Green's function, which only depends on $(d + r)^3$. Further, despite the similar behavior of $q_{\mathrm{E}}$ obtained with this model, and that obtained with the rigorous calculation (compare Figs. 4(c) and 3(b)), some differences still remain. In particular the latter decays more slowly with distance, it changes its sign as the distance increases, and the maximum of $q_{\mathrm{E}}$ is found at a similar distance $d$ for all radii. Moreover, the current model, given by Eqs. (27)–(30), is clearly insufficient to reproduce the exact $q_{\mathrm{R}}$ contribution (compare Figs. 4(c) and 3(a)).

#### 3.3.5. Full retarded Green's function

In order to further approach the exact response of the interacting system, we replace the quasistatic near-field Green's function in Eqs. (26)–(30) with the full expression [40] of the Green's function $G^{\mathrm{F}}_{x,x}$. $G^{\mathrm{qs}}_{x,x} = 1/[(2\pi)\varepsilon_0(r+d)^3]$ (Eq. (20)) is always a real number but $G^{\mathrm{F}}_{x,x}$ is complex, with a phase that changes with distance $d$ largely due to the retardation phase associated with the propagation of the fields. Furthermore, $G^{\mathrm{F}}_{x,x}$ decays more slowly than $G^{\mathrm{qs}}_{x,x}$ with $d$ because it includes terms decaying as $1/(r+d)$ and $i/(r+d)^2$ (corresponding to the far- and intermediate-field contributions, respectively). These changes directly affect the phase and the modulus of the enhancement factor ($K = G^{\mathrm{F}}_{x,x}p_{\mathrm{a}}/E_0$) and thus both $q_{\mathrm{E}}$ and $q_{\mathrm{R}}$ (Eq. (12)), as shown in Fig. 4(d) (fourth column).

We first observe that the distance-dependence of the amplitude and phase of $K$ induces the change of sign of $q_{\mathrm{E}}$ for $d \approx 150$ nm (change from red to blue color), and also the overall slower decay of its absolute value ($|q_{\mathrm{E}}|$) with $d$ discussed above. We show in section S5 of Supplement 1 that $q_{\mathrm{E}}$ oscillates for larger separation distances. The maxima values of $q_{\mathrm{E}}$ are larger than those in the previous model, mainly due to the far- and intermediate field contributions.

Further, we obtain clearly larger values of $|q_{\mathrm{R}}|$ than in the previous model, with values of up to $|q_{\mathrm{R}}| \approx 0.45$, as compared to $|q_{\mathrm{R}}| \lesssim 0.14$ in Fig. 4(c). According to Eq. (13) we can directly relate these high values of $q_{\mathrm{R}}$ to changes of phase of the field enhancement, $\varphi_{\mathrm{A}}$. When the full Green's function $G^{\mathrm{F}}_{x,x}$ is used, $\varphi_{\mathrm{A}}$ can considerably differ from $\pi/2$ for moderate and large $d$, which explains the relatively large values of $|q_{\mathrm{R}}|$. $|q_{\mathrm{R}}|$ is maximum for $(r + d) \approx 100$ nm and it decays

Optics EXPRESS

for larger distances because the field enhancement becomes very small and, thus, $|q_R| \propto |K|^2/\gamma'$ (Eq. (13)) progressively approaches zero.

The asymmetry contributions $q_E$ and $q_R$ take similar absolute values of opposite signs at intermediate distances (20 nm $<d<$100 nm). As a consequence, the total asymmetry $q = q_E + q_R$ partially cancels in this regime, specially for radius 25 nm $\lesssim r \lesssim$ 70 nm. Thus, $q$ presents a saddle point centered at $r \approx 40$ nm and $d \approx 80$ nm. The qualitative dependence of $q$ with radius and distance within this model is in good agreement with the rigorous Mie's theory results (Fig. 2(d)). We thus conclude that this improved model contains the fundamental elements to capture the main features of the behavior of the total asymmetry factor.

#### 3.3.6. Experimental permittivity

We can further increase the agreement with the Mie's theory calculation by using the experimental values $\varepsilon_a^{Exp}$ of the permittivity of silver, as taken from Ref. [36], instead of the modified Drude model. The polarizability of the nanoantenna then becomes $\alpha_a^{RC\text{-}Exp} = \alpha_a^{Exp}(1/1-i(k^3/6\pi\varepsilon_0)\alpha_a^{Exp})$ with $\alpha_a^{Exp} = 4\pi r^3(\varepsilon_a^{Exp}-1)/(\varepsilon_a^{Exp}+2)$. Figure 4(e) (fifth column) shows the asymmetry contributions calculated with this assumption. The changes as compared with the previous model (Fig. 4(d)) are relatively small, and are mostly found for small spheres ($r<$25 nm), where we find an increase of $|q_E|$ and a decrease of $|q_R|$. Indeed, smaller spheres resonate at shorter wavelengths, for which the contribution of the $d$-electrons to the experimental permittivity significantly modifies the plasmonic response. The changes on the asymmetry due to the influence of the $d$-electrons can be larger in other materials. For example, in section S5 of Supplement 1, we show that including this effect is crucial to accurately describe the asymmetry factor for a QE interacting with a gold nanoantenna.

#### 3.3.7. Improved description of the radiative correction

Last we introduce a more accurate description of the radiative–corrected polarizability following Ref. [57]:

$$\alpha_a^{IRC} = \frac{\alpha_a^{Exp}}{1 - \frac{3}{5}x^2\frac{\varepsilon_a^{Exp}-2}{\varepsilon_a^{Exp}+2} - i\alpha_a^{Exp}\frac{(2\pi/\lambda)^3}{6\pi\varepsilon_0} - 3\frac{x^4}{350}\frac{(\varepsilon_a^{Exp})^2-24\varepsilon_a^{Exp}+16}{\varepsilon_a^{Exp}+2}} \tag{31}$$

with $x = 2\pi r/\lambda$.

We implement this improvement to the dipole-dipole interaction model, which can be summarized in a set of equations as:

$$p_a = \alpha_a^{IRC}(E_0 + G^F_{x,x}p_e), \tag{32}$$

$$p_e = \alpha_e(E_0 + K), \tag{33}$$

$$KE_0 = G^F_{x,x}p_a, \tag{34}$$

$$\gamma' = \left[1 + \mathrm{Im}\left\{\frac{A_e\alpha_a^{IRC}}{\gamma\omega_0}(G^F_{x,x})^2\right\}\right]\gamma, \tag{35}$$

$$\sigma_{Ext} = \frac{2\pi}{\lambda\varepsilon_0}\mathrm{Im}\left\{\frac{p_a + p_e}{E_0}\right\}. \tag{36}$$

For ease of reference, we summarize all the aspects that are included in Eqs. (32)–(36) but not in Eqs. (21)–(25) (the latter corresponding to the simplest model considered in this section): i) the direct excitation and emission of the QE are included in Eqs. (33) and (36), respectively, ii) the propagation of the fields beyond the quasistatic approximation is included by the full Green's function in Eqs. (32), (34), and (35), and iii) we use a modified version of the polarizability of the spherical nanoparticle $\alpha_a^{IRC}$ in Eqs. (32) and (35) that incorporates the effect of the radiation

Optics EXPRESS

damping of the nanoantenna and considers the influence of $d$-electrons on the permittivity of the material.

Figure 4(f) (sixth column) shows that by introducing the improved radiative correction (Eq. (31)) the values of the asymmetry change very little, with the largest changes occurring for $r$>50 nm (as compared to the results of the previous model in Fig. 4(e)). In particular the maxima of $|q_{\mathrm{R}}|$ and $q_{\mathrm{E}}$ for $r$>50 nm have been displaced in Fig. 4(f) towards slightly larger distances $d$. The reason for this displacement is that the new radiative correction redshifts the resonant wavelength for large particles, which changes the ratio between the QE-nanoantenna distance and the wavelength, $(r+d)/\lambda$ (affecting the full Green's function $G^{\mathrm{F}}_{x,x}$).

The resulting values of the total asymmetry factor $q$ and the $q_{\mathrm{R}}$ and $q_{\mathrm{E}}$ contributions that are obtained within this improved model (Fig. 4(f)) are in very good agreement with the exact results shown in Figs. 2(d) and 3(a)-(b) for the radius and distances considered. The main difference occurs in the shortest range of distances, $d$<10 nm. For such distances the Mie's theory calculation results in a very large increase of the decay rate $\gamma'$ due to the coupling with the high-order modes of the plasmonic response [49], which is not included in the dipole-dipole description analyzed here. The large increase of $\gamma'$ strongly reduces the asymmetry by increasing the denominator in Eq. (12). However, this decrease is hard to appreciate in the figures, as the value of $q$ predicted by the most refined dipole-dipole interaction model (Eqs. (33)–(36)) is already small for these short distances.

Equations (33)–(36) allow for a simple quantitative description of the total asymmetry factor that enables to identify the different effects that influence the value of $q$. However, it is instructive to further analyze the importance of the radiative correction. In the discussion above, the introduction of the simpler radiative correction only led to a very small change of the asymmetry (compare Fig. 4(a) and Fig. 4(b)), but this effect is small only when considering very simple dipole-dipole interaction models. If the radiative correction is neglected in the final expressions (Eqs. (33)–(36)) we obtain a completely inaccurate response for the total asymmetry factor (and its contributions). This can be observed by comparing Fig. 4(g) (seventh column) with Fig. 4(f), where the only difference between the two is that Fig. 4(g) ignores the radiative correction. We have verified that including the radiative correction is necessary for all the models that use the full Green's function.

We have thus shown, in this section, how each approximation in the dipole-dipole interaction affects the description of the Fano asymmetry for zero-detuning. This has allowed us to associate the different aspects of the asymmetry with relevant physical effects.

## 4. Fano resonance in dimers

In the previous sections we have analyzed in detail the asymmetry of the Fano lineshape that is revealed in the extinction cross section spectrum of a QE placed near a spherical metallic nanoparticle (Fig. 1(a)), chosen as an example of a canonical nanoantenna. To demonstrate that a similar analysis can be applied to more general nanostructures, we consider next the Fano asymmetry for a QE situated in a junction between two spherical gold nanoparticles (a dimer nanoantenna). This dimer configuration has been intensely studied because it induces a much larger near–field enhancement than the single spherical nanoparticle, as sought, for example, in surface-enhanced spectroscopy [4,5,61–66].

We show in Fig. 5(a) a scheme of the dimer configuration. The system is driven by an incident plane wave of amplitude $E_0$ that propagates along the $z$-axis, and polarized along the $x$-axis parallel to the orientation of the point-like dipole that represents the QE and to the axis of symmetry of the two spherical nanoparticles. We consider gold instead of silver nanoparticles in this section. Despite having larger absorption losses, gold is widely used in surface-enhanced spectroscopy because it does not oxidize and it is more handleable in experiments. The permittivity of gold is taken from Johnson and Christy [36], the two spherical nanoparticles have a radius of $r$ = 40

Optics EXPRESS

nm, and we vary their surface-to-surface distance $2d$. The emitter is placed in the middle of the gap between the two nanoparticles (at distance $d$ from the surface of each of them), and its properties are the same as in the previous sections (strength $\mu = 0.05$ $e$·nm, intrinsic decay rate corresponding to the spontaneous radiative decay, and resonance frequency tuned as a function of $d$ to always match the dipolar resonance of the nanoantenna [67]), *i.e.*, we keep the condition of zero-detuning in all cases analyzed and shown here.

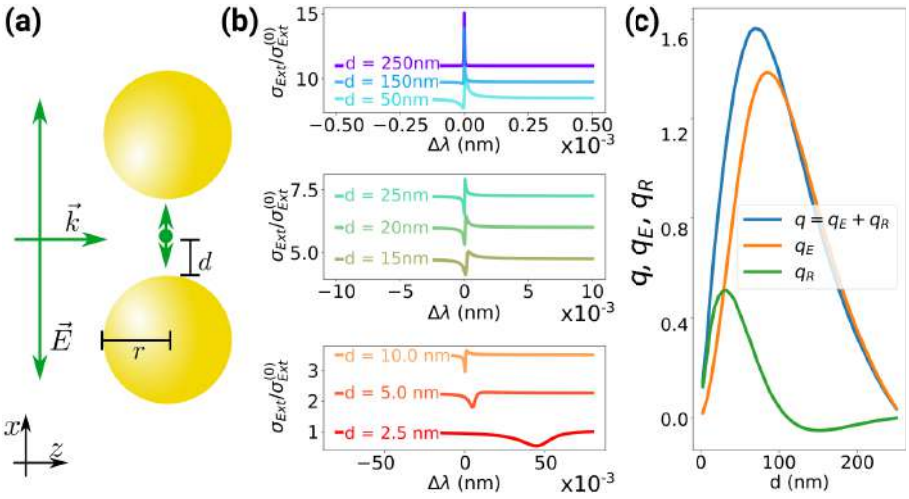


**Fig. 5.** Characterization of the Fano asymmetry in the extinction cross–section of a QE coupled to a metallic dimer obtained at zero detuning (resonant conditions). (a) Scheme of the dimer nanostructure. A QE with dipole momentum polarized along the $x$-axis is placed between two gold spherical nanoparticles of radius $r = 40$ nm at a distance $d$ from the surface of each of them (the separation between the center of the two nanoparticles is $2(d + r)$). The dimer axis is parallel to the $x$-axis. The system is illuminated by a plane wave propagating along the $z$-axis and with the electric field polarized along the $x$-axis. (b) Normalized extinction cross-section spectra $\sigma_{\rm Ext}/\sigma^{(0)}_{\rm Ext}$ of the coupled emitter-dimer nanoantenna system. The spectra are vertically displaced by 1.5 for clarity. Each Fano lineshape is evaluated for different values of $d$ that range from $d = 2.5$ nm to $d = 250$ nm (see labels in the figure). The spectra are grouped in three separate panels, each of them plotted over a different spectral range, $\Delta\lambda$. (c) Dependence with distance $d$ of the Fano total asymmetry factor $q$ (blue line) together with its contributions $q_{\rm E}$ (orange line) and $q_{\rm R}$ (green line). For each separation distance $d$ of the calculations in (b) and (c) we have set the resonance of the QE to match the frequency of resonance of the nanoantenna.

Figure 5(b) shows the extinction cross-section spectrum of this hybrid system calculated for different values of $d$, as obtained from the solution of Maxwell's equations using the Matlab package *MNPBEM17* [68–70] (the details of these calculations are given in the section S4 of Supplement 1). A clear Fano feature is observed in all spectra, showing a qualitatively similar dependence with distance as the results of the single spherical nanoparticle (Fig. 1(c)). In both situations the Fano lineshape obtained at small distances $d \lesssim 10$ nm corresponds to a broadened and almost symmetric dip, while at much larger separation distances, $d \gtrsim 200$ nm, we observe an almost symmetric narrow peak. Thus, $q \approx 0$ in these two situations. For values of $d$ between these two extremes, the Fano spectrum shows various degrees of asymmetry.

Despite these qualitative similarities, the results obtained for the dimer nanoantenna (Fig. 5(b)) and a single silver nanoparticle (Fig. 1(c)) show some clear quantitative differences. For instance, the Purcell factor $P_{\rm F}$ and the photonic Lamb shift $\Delta\omega$ experienced by the emitter, which describe

Optics EXPRESS

the broadening and shift of the Fano feature, respectively, are much larger in the case of the dimer due to the stronger field confinement [4,61,66] ($P_F \approx 1.4 \times 10^4$ and $\Delta\omega/\gamma \approx 3.2 \times 10^5$ for the dimer and $d = 2.5$ nm, to be compared with $P_F \approx 4.3 \times 10^2$ and $\Delta\omega/\gamma \approx 4.4 \times 10^3$ for the single silver spherical nanoparticle system of the same radius $r$ and distance $d$). We also observe that there is a clear asymmetry for a larger range of distances in the dimer as compared to the single silver nanoantenna of the same radius (compare the three panels in Fig. 5(b) and Fig. 1(c))

To study the Fano asymmetry of the dimer system in more detail, we show in Fig. 5(c) the dependence with $d$ of the total asymmetry factor $q$ (blue line) and its two components $q_E$ (orange line) and $q_R$ (green line), as obtained from Eq. (12) (with $q = q_E + q_R$). For separation distances $d \gtrsim 30$ nm the total asymmetry factor $q$ is mainly influenced by the $q_E$ contribution, *i.e.* it is mostly due to the direct excitation and emission of the QE. In a similar way as for the single spherical nanoparticle, $q_E$ is larger at intermediate distances (20 nm $\lesssim d \lesssim$ 200 nm for the dimer), when the excitation and emission of the QE via the nanoantenna has a magnitude comparable to the direct excitation by the incident plane wave and the direct emission of the QE to the far field, respectively. Outside this range of distances this condition is not verified and $q_E$ is small.

On the other hand, the $q_R$ contribution (green line in Fig. 5(c)) dominates the total asymmetry factor for $d \lesssim 30$ nm. The distance dependence of $q_R$ can again be explained using Eq. (13), which indicates that $q_R \propto |K|^2 \sin(2\varphi_A)/\gamma'$. The $|K|^2/\gamma'$ factor in this expression explains many aspects of the general tendency of $|q_R|$. For long separation distances, $d \gtrsim 200$ nm, the field-enhancement factor $|K|$ approaches zero, leading to small values of $|q_R|$. For short distances $d \lesssim 10$ nm the quenching induced by the coupling of the emitter with the high–order modes of the plasmonic dimer also becomes important [49]. As a consequence, the plasmon-enhanced decay rate $\gamma' = (1 + P_F)\gamma$ takes significantly higher values than the enhancement of the intensity $|K|^2$, leading to small values of $|q_R|$. Between these two regimes of $d$, $|K|^2/\gamma'$ is maximized, so that $|q_R|$ can be relatively large. Additionally, $q_R$ is also influenced by the phase $\varphi_A$ of the enhancement, which changes with distance largely due to propagation effects. The resulting $\sin(2\varphi_A)$ factor has an oscillatory behaviour with the separation distance with an approximated period of 200 nm, and the changes of sign are directly reflected in the oscillation of $q_R$, as shown in Fig. 5(c) (green line). Further, $\sin(2\varphi_A)$ decreases sharply if the distance becomes smaller than $d \lesssim 10$ nm, emphasizing the rapid decrease of $q_R$ for this range of distances.

Overall the general trends of $|q_R|$ obtained for the dimer system as a function of separation distance $d$ (Fig. 5(c)) resemble the result obtained for the silver spherical nanoparticle (Fig. 3(a)), both showing a clear maximum for intermediate distances. However, some significant differences can be pointed out. The range of distances where $|q_R|$ is large extends towards significantly smaller $d$ in the case of the gold dimer ($|q_R|>0.25$ for 10 nm $\lesssim d \lesssim$ 70 nm) as compared to the single silver spherical nanoparticle ($|q_R|>0.25$ for 40 nm $\lesssim d \lesssim$ 80 nm and $r = 40$ nm). Further, $q_R$ takes relatively large positive values in the dimer structure ($d \lesssim 100$ nm in Fig. 5(c)), in contrast to the negative values of $q_R$ calculated for the single spherical nanoparticle of the same radius ($d \lesssim 100$ nm in Fig. 3(c)). This last difference mostly occurs due to the stronger influence of the $d$-electrons in the permittivity of gold (used for the dimer material) as compared to silver (for the response of a single gold spherical nanoparticle, see section S5 of Supplement 1). The contribution of the $d$-electrons significantly modifies the phase of the field enhancement $\varphi_A$, and thus the asymmetry.

## 5. Summary and conclusions

We analyze in detail the asymmetry of the Fano feature found in the extinction cross-section spectrum of a nanoantenna interacting with a QE resonantly, *i.e.* the QE and the nanoantenna have the same resonant excitation frequency, and thus, the asymmetry is not due to the detuning. We have focused on the coupling with an exciton of a single QE but the conclusions also apply to coupling with many QEs or with molecular vibrations. We first consider a spherical

Optics EXPRESS

silver nanoantenna under laser illumination as a canonical nanoantenna. We show that the spectra obtained with exact electromagnetic calculations of the optical response of the hybrid QE-nanoantenna system under zero detuning present an asymmetry not found in a very simple dipole-dipole interaction description.

The asymmetry of the Fano feature is quantified through a parameter $q$. We derive an analytical expression of $q$ that depends mainly on the field-enhancement and the plasmon-enhanced losses of the QE. This expression can be decomposed into two contributions, $q = q_{\mathrm{E}} + q_{\mathrm{R}}$, where $q_{\mathrm{E}}$ is mainly connected with the direct emission and excitation of the QE, while $q_{\mathrm{R}}$ mostly captures other phenomena (such as retardation) that affect the phase of the field enhancement that the nanoantenna induces on the QE.

The analytical expression of $q$ evaluated with different dipole-dipole interaction models (with an increasing degree of complexity) allow us to analyze in detail the origin of the asymmetry. These models improve the description of the polarizability of the spherical nanoparticle and that of the Green's function that governs the QE-nanoantenna interaction. The implementation of these models enables to identify the influence of five effects on the asymmetry: i) the radiation damping of the nanoantenna, which makes it necessary to introduce a radiative correction to its response. Ignoring this correction results in an completely unreliable description of the optical response of large nanoparticles and thus of the resulting asymmetry; ii) the influence of $d$-electrons on the permittivity of the plasmonic material, and thus of the polarizability of the nanoantenna. This contribution is particularly important for nanoantennas that resonate at shorter wavelengths (for example, small spherical nanoparticles); iii) the direct excitation of the QE by the incident field exciting the system and the direct emission of the QE to the far-field, *i.e.* the two contributions to the $q_{\mathrm{E}}$ asymmetry factor discussed above; iv) the propagation of the fields beyond the quasistatic near-field approximation. The asymmetry can be affected by the slowly-decaying terms of the vacuum Green's function (intermediate and far-field terms) and, especially, by the retardation-induced changes of the phase of the fields induced by the nanoantenna at the position of the emitter (and vice–versa); v) the changes of the optical response of the nanoantenna due to its high–order modes. The high–order modes of the nanoantenna are not included in the dipole-dipole interaction models analyzed in this work, but their influence is revealed by comparing our most complete dipole-dipole interaction model with the rigorous calculations. These rigorous calculations show reduced values of the asymmetry for short distances between the QE and the nanoantenna due to the quenching induced by the coupling of the QE exciton to the high-order plasmonic modes of the nanoantenna [49].

Further, we note that although the effect of the high-order modes for moderate and large separation distances is relatively small for a single nanoantenna under laser illumination, it could be more important when the illumination is a point-like source (tunneling current or a transition dipole moment in a molecule) that can couple very efficiently to highly-confined modes. This aspect could explain, for instance, the asymmetry observed in recent experiments that analyzed the emission spectrum of a QE placed in a plasmonic nanocavity formed between the metallic tip of a scanning tunneling microscope and a metallic substrate, with the system being excited by the localized fluctuation of the tunneling current at optical frequencies [14].

Last, we show that the asymmetry analysis can also be applied to more complex nanostructures. Specifically, we show that the modifications of the Fano features obtained for the single silver spherical nanoantenna is similar to the results obtained for a gold dimer nanoantenna, with some quantitative differences. As an example of these differences, the asymmetry contribution $q_{\mathrm{R}}$ is mainly positive for the gold dimer system and mainly negative of the single silver spherical nanoparticle (of the same radius), which is mostly due to the larger influence of the $d$-electrons in the permittivity of gold. However, we emphasize that the effects behind the origin of the asymmetry are similar in both systems. Thus we conclude that the analysis proposed in this

Optics EXPRESS

work provides insights into the origin of the asymmetry of the Fano lineshape applicable to very general systems in nanophotonics.

## Appendix A: origin of the Fano asymmetry as an interference effect

In this appendix we discuss how the asymmetry in the Fano lineshape of the extinction spectra can be understood in terms of the phases of the different contributions to the scattered electric field (or far-field), as sketched in Fig. 6 [26]. With this aim, we only need to consider the field scattered in the forward direction $E_x^{\mathrm{d}}$, which directly gives the extinction cross-section according to the optical theorem [39] ($\sigma_{\mathrm{Ext}} = 2\lambda \mathrm{Im}\{z_{\mathrm{d}} e^{-i2\pi z_{\mathrm{d}}/\lambda} E_x^{\mathrm{d}}/E_0\}$, with $z_{\mathrm{d}}$ the distance from the center of mass of the nanoantenna to the detector).

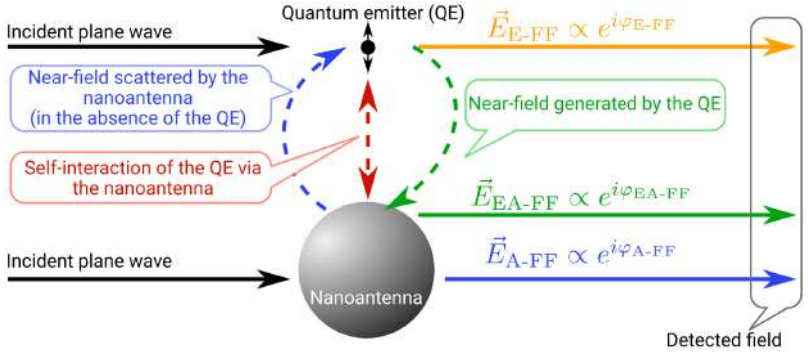


**Fig. 6.** Scheme of the scattering process for our system. The incident plane wave (black arrows) illuminate the QE and the nanoantenna. The nanoantenna scatters the incident light directly (in the absence of the QE) to the far-field (solid blue arrow), and it also generates a near-field that excites the exciton of the QE (dashed blue arrow). The excited QE generates a field on the nanoantenna that is scattered back to itself, causing a self-interaction (dashed red arrow), and a modification on the induced dipole moment on the QE. The self-consistently excited QE emits directly (in the absence of the nanoantenna) to the far-field (solid orange arrow) and also excites the nanoantenna (green dashed arrow). The field induced by the QE on the nanoantenna is also scattered to the far-field (solid green arrow).

We first consider the scenario where the plane-wave illumination only excites the nanoantenna. In this scenario, the QE is only driven by the near field induced by the nanoantenna (dashed blue arrow in Fig. 6), *i.e.*, we ignore the direct excitation of the QE by the plane wave (an approximation often valid in plasmonic systems). Moreover, in this initial scenario, we also ignore the direct emission by the exciton of the QE (solid orange arrow). Thus, we can distinguish between two contributions to the scattered electric field at the detector: the scattering of the nanoantenna in the absence of the QE, $\vec{E}_{\mathrm{A\text{-}FF}}$ (solid blue arrow), and the scattered field by the nanoantenna due to its excitation by the QE, $\vec{E}_{\mathrm{EA\text{-}FF}}$ (solid green arrow). In simple scenarios, we can predict the spectral symmetry of the Fano feature by analyzing the phase of these two contributions to the total far-field emission.

To analyze the phases $\varphi_{\mathrm{A\text{-}FF}}$ and $\varphi_{\mathrm{EA\text{-}FF}}$ of the respective far-field contributions, $\vec{E}_{\mathrm{A\text{-}FF}}$ and $\vec{E}_{\mathrm{EA\text{-}FF}}$, we connect them with the phases of the near-field interactions between the antenna and the QE. First, in the absence of the QE, the nanoantenna is only excited by the incident plane wave and it generates a near field at the QE position, $\vec{E}_{\mathrm{A\text{-}NF}}$ (dashed blue arrow in the figure). $\vec{E}_{\mathrm{A\text{-}NF}}$ has a phase $\varphi_{\mathrm{A\text{-}NF}} = \varphi_{\mathrm{A\text{-}FF}} - \delta_{\mathrm{FF}} + \delta_{\mathrm{NF}}$, where $\delta_{\mathrm{FF}} = 2\pi z_{\mathrm{d}}/\lambda$ is the propagation phase from the center of mass of the antenna to the detector. $\delta_{\mathrm{NF}} = \varphi_{\mathrm{A\text{-}NF}} - (\varphi_{\mathrm{A\text{-}FF}} - \delta_{\mathrm{FF}})$ is the difference between $\varphi_{\mathrm{A\text{-}NF}}$, the phase of the near field generated by the bare nanoantenna at the position of the QE and $(\varphi_{\mathrm{A\text{-}FF}} - \delta_{\mathrm{FF}})$, the phase of the far-field emission of the bare antenna subtracting the

Optics EXPRESS

phase acquired due to propagation, $\delta_{\text{FF}}$. $\delta_{\text{NF}}$ can include effects such as the near-field contribution of high-order modes supported by the nanoantenna. However, in a simple scenario where an electric dipole mode dominates the behavior of the nanoantenna, $\delta_{\text{NF}}$ is directly given by $\delta_{\text{P}}$, the phase acquired by the field propagation from the nanoantenna to the QE.

On the other hand, the fields scattered by the nanoantenna induce a dipole moment at the QE with phase $\varphi_{\text{A-NF}} + \varphi_{\text{E}} + \varphi_{\text{SI}}$, where $\varphi_{\text{A-NF}}$ is the phase of the fields scattered by the nanoantenna in the absence of the QE as described above, and $\varphi_{\text{E}}$ is the phase of the polarizability of the bare QE. The $\varphi_{\text{SI}}$ phase is included to take into account that the field scatters back onto the QE. This self-interaction of the QE (dasher red-line in the figure) can be modeled as a modification of the polarizability of the QE (see section S1 of Supplement 1), which adds the $\varphi_{\text{SI}}$ phase to the response of the bare QE. The dipole moment induced at the QE, generates a field at the center of the nanoantenna $\vec{E}_{\text{EA-NF}}$ (dashed green line in the figure) with phase $\varphi_{\text{EA-NF}} = \varphi_{\text{A-NF}} + \varphi_{\text{E}} + \varphi_{\text{SI}} + \delta_{\text{P}}$.

The near-field $\vec{E}_{\text{EA-NF}}$ excites the nanoantenna, which later scatters to the far-field giving the $\vec{E}_{\text{EA-FF}}$ contribution with a phase

$$\varphi_{\text{EA-FF}} = \varphi_{\text{EA-NF}} + \varphi_{\text{A-FF}} + \delta'_{\text{NF}}. \tag{37}$$

$\delta'_{\text{NF}}$ is the difference in phase in the emission of the bare nanoantenna to the far field between a situation when it is excited with a plane wave and when excited by a point-like dipole (with the same phase). In the situation where the emission is equal in the direction towards the detector and the direction toward the source of the excitation (as all systems considered here), we then can apply reciprocity [53–55] and obtain $\delta'_{\text{NF}} = \delta_{\text{NF}}$.

The difference between the phase $\varphi_{\text{EA-FF}}$ of the $\vec{E}_{\text{EA-FF}}$ contribution and the phase $\varphi_{\text{A-FF}}$ of $\vec{E}_{\text{A-FF}}$ leads to constructive or destructive interference, which gives the Fano feature. For example, the symmetric Fano dips obtained under resonant conditions in Fig. 1(b) for the simple dipole-dipole interaction model (introduced in section 2) are due to perfect destructive interference between $\vec{E}_{\text{EA-FF}}$ and $\vec{E}_{\text{A-FF}}$ at resonance (*i.e.*, $\varphi_{\text{A-FF}} - \varphi_{\text{EA-FF}} = \pi$ for resonant illumination). This condition is fulfilled because, within this model, the $\delta_{\text{NF}}$ phase directly corresponds to the phase of the near-field propagation $\delta_{\text{NF}} = \delta_{\text{P}}$, and $\delta_{\text{P}} = 0$ due to the quasistatic approximation assumed in the simple dipole-dipole interaction model, which also causes the self-interaction to have a zero phase ($\varphi_{\text{SI}} = 0$). Furthermore, in the simple dipole-dipole interaction model, the phase of $\vec{E}_{\text{A-FF}}$ is $\varphi_{\text{A-FF}} = \varphi_{\text{A}} + \delta_{\text{FF}}$, where $\varphi_{\text{A}}$ is the phase of the polarizability of the nanoantenna. Finally, this model considers that the polarizability of the nanoantenna and of the QE (Eqs. (3) and (4)) are purely imaginary at resonance ($\varphi_{\text{A}} = \pi/2$ and $\varphi_{\text{E}} = \pi/2$). Thus, by considering all these effects, we obtain that, $\varphi_{\text{A-FF}} = \pi/2 + \delta_{\text{FF}}$ and $\varphi_{\text{EA-FF}} = 3\pi/2 + \delta_{\text{FF}}$, resulting in perfect destructive interference at resonance.

However, when considering the exact response, different phenomena can affect the phase of the fields scattered by the QE and the nanoantenna and, thus, introduce an arbitrary degree of asymmetry of the Fano lineshape even in resonance. For example, the phase of the field directly scattered by the nanoantenna to the far field (minus the propagation to the far-field, $\varphi_{\text{A-FF}} - \delta_{\text{FF}}$), and the phase of the near fields induced by the nanoantenna at the QE ($\varphi_{\text{A-NF}}$) can be different from $\pi/2$. The latter occurs, for instance, when the retardation in the propagation of the fields from the nanoantenna to the QE is considered. Furthermore, the direct excitation of the QE by the incident illumination and the direct emission of the QE, which were neglected above, needs to be considered in the exact calculations. The direct illumination modifies the field exciting the dipole and, thus, its phase. The direct emission of the QE contributes to the total scattered electric field (orange line), introducing an additional interference in the total emission of the system. In Supplement 1, we show that the near field is also strongly affected by similar interference effects.

**Funding.** Department of Education, Research and Universities of the Basque Government (IT-1526-22); Ministerio de Ciencia e Innovación and Agencia Estatal de Investigación (MCIN/AEI/10.13039/501100011033, PID2019-107432GB-I00); Predoctoral MCIN grant BES-2017-080073.

Optics EXPRESS

**Acknowledgements.** Á. N. thanks A. Babaze for many useful inputs and valuable discussions, and M. Urbieta for his help with the *MNPBEM17* simulations.

**Disclosures.** The authors declare no conflict of interest.

**Data availability.** Data underlying the results presented in this paper are not publicly available at this time but may be obtained from the authors upon reasonable request.

**Supplemental document.** See Supplement 1 for supporting content.

## References

1. S. A. Maier, "Effective mode volume of nanoscale plasmon cavities," Opt. Quantum Electron. **38**(1-3), 257–267 (2006).
2. S. Huang, T. Ming, Y. Lin, X. Ling, Q. Ruan, T. Palacios, J. Wang, M. Dresselhaus, and J. Kong, "Ultrasmall mode volumes in plasmonic cavities of nanoparticle-on-mirror structures," Small **12**(37), 5190–5199 (2016).
3. M. Pelton, J. Aizpurua, and G. Bryant, "Metal-nanoparticle plasmonics," Laser Photonics Rev. **2**(3), 136–159 (2008).
4. G. C. Li, Q. Zhang, S. A. Maier, and D. Lei, "Plasmonic particle-on-film nanocavities: a versatile platform for plasmon-enhanced spectroscopy and photochemistry," Nanophotonics **7**(12), 1865–1889 (2018).
5. F. Benz, R. Chikkaraddy, A. Salmon, H. Ohadi, B. de Nijs, J. Mertens, C. Carnegie, R. W. Bowman, and J. J. Baumberg, "Sers of individual nanoparticles on a mirror: Size does matter, but so does shape," J. Phys. Chem. Lett. **7**(12), 2264–2269 (2016).
6. X. Wu, S. K. Gray, and M. Pelton, "Quantum-dot-induced transparency in a nanoscale plasmonic resonator," Opt. Express **18**(23), 23633–23645 (2010).
7. G. M. Akselrod, C. Argyropoulos, T. B. Hoang, C. Ciracì, C. Fang, J. Huang, D. R. Smith, and M. H. Mikkelsen, "Probing the mechanisms of large Purcell enhancement in plasmonic nanoantennas," Nat. Photonics **8**(11), 835–840 (2014).
8. A. F. Koenderink, "Single-photon nanoantennas," ACS Photonics **4**(4), 710–722 (2017).
9. L. Novotny and N. van Hulst, "Antennas for light," Nat. Photonics **5**(2), 83–90 (2011).
10. T. Neuman, C. Huck, J. Vogt, F. Neubrech, R. Hillenbrand, J. Aizpurua, and A. Pucci, "Importance of plasmonic scattering for an optimal enhancement of vibrational absorption in seira with linear metallic antennas," J. Phys. Chem. C **119**(47), 26652–26662 (2015).
11. F. Neubrech, A. Pucci, T. W. Cornelius, S. Karim, A. García-Etxarri, and J. Aizpurua, "Resonant plasmonic and vibrational coupling in a tailored nanoantenna for infrared detection," Phys. Rev. Lett. **101**(15), 157403 (2008).
12. I. Abid, W. Chen, J. Yuan, S. Najmaei, E. C. Pe nafiel, R. Péchou, N. Large, J. Lou, and A. Mlayah, "Surface enhanced resonant raman scattering in hybrid MoSe2@Au nanostructures," Opt. Express **26**(22), 29411–29423 (2018).
13. R. D. Artuso and G. W. Bryant, "Optical response of strongly coupled quantum dot-metal nanoparticle systems: Double peaked fano structure and bistability," Nano Lett. **8**(7), 2106–2111 (2008).
14. Y. Zhang, Q. S. Meng, L. Zhang, Y. Luo, Y. J. Yu, B. Yang, Y. Zhang, R. Esteban, J. Aizpurua, Y. Luo, J. L. Yang, Z.-C. Dong, and J. Hou, "Sub-nanometre control of the coherent interaction between a single molecule and a plasmonic nanocavity," Nat. Commun. **8**(1), 15225 (2017).
15. D. O. Sigle, S. Kasera, L. O. Herrmann, A. Palma, B. de Nijs, F. Benz, S. Mahajan, J. J. Baumberg, and O. A. Scherman, "Observing single molecules complexing with cucurbit[7]uril through nanogap surface-enhanced raman spectroscopy," J. Phys. Chem. Lett. **7**(4), 704–710 (2016).
16. Y. Yu, T. H. Xiao, Y. Wu, W. Li, Q. G. Zeng, L. Long, and Z. Y. Li, "Roadmap for single-molecule surface-enhanced raman spectroscopy," Adv. Photonics **2**(1), 014002 (2020).
17. A. B. Zrimsek, N. Chiang, M. Mattei, S. Zaleski, M. O. McAnally, C. T. Chapman, A.-I. Henry, G. C. Schatz, and R. P. Van Duyne, "Single-molecule chemistry with surface-and tip-enhanced raman spectroscopy," Chem. Rev. **117**(11), 7583–7613 (2017).
18. R. Chikkaraddy, B. de Nijs, F. Benz, S. J. Barrow, O. A. Scherman, E. Rosta, A. Demetriadou, P. Fox, O. Hess, and J. J. Baumberg, "Single-molecule strong coupling at room temperature in plasmonic nanocavities," Nature **535**(7610), 127–130 (2016).
19. D. E. Chang, A. S. Sørensen, E. A. Demler, and M. D. Lukin, "A single-photon transistor using nanoscale surface plasmons," Nat. Phys. **3**(11), 807–812 (2007).
20. J. V. Pellegrotti, E. Cortés, M. D. Bordenave, M. Caldarola, M. P. Kreuzer, A. D. Sanchez, I. Ojea, A. V. Bragas, and F. D. Stefani, "Plasmonic photothermal fluorescence modulation for homogeneous biosensing," ACS Sens. **1**(11), 1351–1357 (2016).
21. F. Madzharova, Á. Nodar, V. Živanovic, M. R. S. Huang, C. T. Koch, R. Esteban, J. Aizpurua, and J. Kneipp, "Gold- and silver-coated barium titanate nanocomposites as probes for two-photon multimodal microspectroscopy," Adv. Funct. Mater. **29**(49), 1904289 (2019).
22. A. Babaze, R. Esteban, J. Aizpurua, and A. G. Borisov, "Second-harmonic generation from a quantum emitter coupled to a metallic nanoantenna," ACS Photonics **7**(3), 701–713 (2020).
23. J. Butet, P. F. Brevet, and O. J. F. Martin, "Optical second harmonic generation in plasmonic nanostructures: From fundamental principles to advanced applications," ACS Nano **9**(11), 10545–10562 (2015).
24. M. R. Singh, "Enhancement of the second-harmonic generation in a quantum dot–metallic nanoparticle hybrid system," Nanotechnology **24**(12), 125701 (2013).

Optics EXPRESS


25. A. E. Miroshnichenko, S. Flach, and Y. S. Kivshar, "Fano resonances in nanoscale structures," Rev. Mod. Phys. **82**(3), 2257–2298 (2010).
26. B. Gallinet, "Fano resonances in plasmonic nanostructures fundamentals, numerical modeling and applications," Ph.D. thesis, École Polytechnique Fédérale De Lausanne, Lausanne (2012).
27. M. F. Limonov, M. V. Rybin, A. N. Poddubny, and Y. S. Kivshar, "Fano resonances in photonics," Nat. Photonics **11**(9), 543–554 (2017).
28. M. Autore, L. Mester, M. Goikoetxea, and R. Hillenbrand, "Substrate matters: surface-polariton enhanced infrared nanospectroscopy of molecular vibrations," Nano Lett. **19**(11), 8066–8073 (2019).
29. K. Tanaka, E. Plum, J. Y. Ou, T. Uchino, and N. I. Zheludev, "Multifold enhancement of quantum dot luminescence in plasmonic metamaterials," Phys. Rev. Lett. **105**(22), 227403 (2010).
30. Y. Moritake, Y. Kanamori, and K. Hane, "Emission wavelength tuning of fluorescence by fine structural control of optical metamaterials with fano resonance," Sci. Rep. **6**(1), 33208 (2016).
31. A. Ahmadivand, B. Gerislioglu, Z. Ramezani, and S. A. Ghoreishi, "Demonstration of robust plexcitonic coupling in organic molecules-mediated toroidal meta-atoms," Adv. Opt. Mater. **7**(24), 1901248 (2019).
32. A. Ahmadivand, "Tunneling plasmonics: vacuum rabi oscillations in carbon nanotube mediated electromigrated nanojunctions," J. Phys. Chem. C **125**(1), 782–791 (2021).
33. A. Lovera, B. Gallinet, P. Nordlander, and O. J. Martin, "Mechanisms of fano resonances in coupled plasmonic systems," ACS Nano **7**(5), 4527–4536 (2013).
34. J. Kundu, F. Le, P. Nordlander, and N. J. Halas, "Surface enhanced infrared absorption (seira) spectroscopy on nanoshell aggregate substrates," Chem. Phys. Lett. **452**(1-3), 115–119 (2008).
35. T. Hartsfield, W.-S. Chang, S. C. Yang, T. Ma, J. Shi, L. Sun, G. Shvets, S. Link, and X. Li, "Single quantum dot controls a plasmonic cavity's scattering and anisotropy," Proc. Natl. Acad. Sci. **112**(40), 12288–12292 (2015).
36. P. B. Johnson and R. W. Christy, "Optical constants of the noble metals," Phys. Rev. B **6**(12), 4370–4379 (1972).
37. M. Pelton, S. D. Storm, and H. Leng, "Strong coupling of emitters to single plasmonic nanoparticles: exciton-induced transparency and rabi splitting," Nanoscale **11**(31), 14540–14552 (2019).
38. E. Kamenetskii, A. Sadreev, and A. Miroshnichenko, *Fano resonances in optics and microwaves* (Springer, 2018).
39. C. Bohren and D. Huffman, *Absorption and Scattering of Light by Small Particles* (Wiley, 1983).
40. L. Novotny and B. Hecht, *Principles of Nano-Optics* (Cambridge University Press, 2006).
41. W. E. Lamb and R. C. Retherford, "Fine structure of the hydrogen atom by a microwave method," Phys. Rev. **72**(3), 241–243 (1947).
42. E. M. Purcell, "Spontaneous emission probabilities at radio frequencies," Phys. Rev. **69**, 839 (1946).
43. M. V. Rybin, S. F. Mingaleev, M. F. Limonov, and Y. S. Kivshar, "Purcell effect and lamb shift as interference phenomena," Sci. Rep. **6**(1), 20599 (2016).
44. R. Esteban, T. V. Teperik, and J. J. Greffet, "Optical patch antennas for single photon emission using surface plasmon resonances," Phys. Rev. Lett. **104**(2), 026802 (2010).
45. K. Joulain, R. Carminati, J. P. Mulet, and J. J. Greffet, "Definition and measurement of the local density of electromagnetic states close to an interface," Phys. Rev. B **68**(24), 245405 (2003).
46. D. J. Heinzen and M. S. Feld, "Vacuum radiative level shift and spontaneous-emission linewidth of an atom in an optical resonator," Phys. Rev. Lett. **59**(23), 2623–2626 (1987).
47. J. M. Wylie and J. E. Sipe, "Quantum electrodynamics near an interface. II," Phys. Rev. A **32**(4), 2030–2043 (1985).
48. H. Walther, B. T. H. Varcoe, B. G. Englert, and T. Becker, "Cavity quantum electrodynamics," Rep. Prog. Phys. **69**(5), 1325–1382 (2006).
49. P. Anger, P. Bharadwaj, and L. Novotny, "Enhancement and quenching of single-molecule fluorescence," Phys. Rev. Lett. **96**(11), 113002 (2006).
50. B. Gurlek, V. Sandoghdar, and D. Martín-Cano, "Manipulation of quenching in nanoantenna-emitter systems enabled by external detuned cavities: A path to enhance strong-coupling," ACS Photonics **5**(2), 456–461 (2018).
51. D. C. Marinica, H. Lourenço-Martins, J. Aizpurua, and A. G. Borisov, "Plexciton quenching by resonant electron transfer from quantum emitter to metallic nanoantenna," Nano Lett. **13**(12), 5972–5978 (2013).
52. J. D. Jackson, *Classical electrodynamics* (Wiley, New York, NY, 1999).
53. R. Carminati, M. Nieto-Vesperinas, and J. J. Greffet, "Reciprocity of evanescent electromagnetic waves," J. Opt. Soc. Am. A **15**(3), 706–712 (1998).
54. P. Bharadwaj, B. Deutsch, and L. Novotny, "Optical antennas," Adv. Opt. Photonics **1**(3), 438–483 (2009).
55. R. Esteban, M. Laroche, and J. Greffet, "Influence of metallic nanoparticles on upconversion processes," J. Appl. Phys. **105**(3), 033107 (2009).
56. C. Balanis, *Antenna Theory: Analysis and Design* (Wiley, 2015).
57. D. Schebarchov, B. Auguié, and E. C. Le Ru, "Simple accurate approximations for the optical properties of metallic nanospheres and nanoshells," Phys. Chem. Chem. Phys. **15**(12), 4233–4242 (2013).
58. E. C. Le Ru, W. R. C. Somerville, and B. Auguié, "Radiative correction in approximate treatments of electromagnetic scattering by point and body scatterers," Phys. Rev. A **87**(1), 012504 (2013).
59. J. Zuloaga and P. Nordlander, "On the energy shift between near-field and far-field peak intensities in localized plasmon systems," Nano Lett. **11**(3), 1280–1283 (2011).

Optics EXPRESS


60. J. Chen, P. Albella, Z. Pirzadeh, P. Alonso-González, F. Huth, S. Bonetti, V. Bonanni, J. Åkerman, J. Nogués, P. Vavassori, A. Dmitriev, J. Aizpurua, and R. Hillenbrand, "Plasmonic nickel nanoantennas," Small **7**(16), 2341–2347 (2011).
61. J. J. Baumberg, J. Aizpurua, M. H. Mikkelsen, and D. R. Smith, "Extreme nanophotonics from ultrathin metallic gaps," Nat. Mater. **18**(7), 668–678 (2019).
62. F. Benz, C. Tserkezis, L. O. Herrmann, B. de Nijs, A. Sanders, D. O. Sigle, L. Pukenas, S. D. Evans, J. Aizpurua, and J. J. Baumberg, "Nanooptics of molecular-shunted plasmonic nanojunctions," Nano Lett. **15**(1), 669–674 (2015).
63. I. Romero, J. Aizpurua, G. W. Bryant, and F. J. G. de Abajo, "Plasmons in nearly touching metallic nanoparticles: singular response in the limit of touching dimers," Opt. Express **14**(21), 9988–9999 (2006).
64. L. Mao, Z. Li, B. Wu, and H. Xu, "Effects of quantum tunneling in metal nanogap on surface-enhanced raman scattering," Appl. Phys. Lett. **94**(24), 243102 (2009).
65. J. Zuloaga, E. Prodan, and P. Nordlander, "Quantum description of the plasmon resonances of a nanoparticle dimer," Nano Lett. **9**(2), 887–891 (2009).
66. C. Lumdee, B. Yun, and P. G. Kik, "Gap-plasmon enhanced gold nanoparticle photoluminescence," ACS Photonics **1**(11), 1224–1230 (2014).
67. R. T. Hill, J. J. Mock, A. Hucknall, S. D. Wolter, N. M. Jokerst, D. R. Smith, and A. Chilkoti, "Plasmon ruler with angstrom length resolution," ACS Nano **6**(10), 9237–9246 (2012).
68. U. Hohenester and A. Trügler, "MNPBEM - A Matlab toolbox for the simulation of plasmonic nanoparticles," Comput. Phys. Commun. **183**(2), 370–381 (2012).
69. U. Hohenester, "Simulating electron energy loss spectroscopy with the MNPBEM toolbox," Comput. Phys. Commun. **185**(3), 1177–1187 (2014).
70. J. Waxenegger, A. Trügler, and U. Hohenester, "Plasmonics simulations with the mnpbem toolbox: Consideration of substrates and layer structures," Comput. Phys. Commun. **193**, 138–150 (2015).